

## Simple PEG Conjugation of SPIO via an Au–S Bond Improves Its Tumor Targeting Potency as a Novel MR Tumor Imaging Agent

Hiroki Kojima,<sup>†</sup> Yohei Mukai,<sup>\*†</sup> Mai Yoshikawa,<sup>†</sup> Kazumasa Kamei,<sup>†</sup> Tomoaki Yoshikawa,<sup>†</sup> Masahito Morita,<sup>‡,§</sup> Toshiro Inubushi,<sup>§</sup> Takao A Yamamoto,<sup>||</sup> Yasuo Yoshioka,<sup>†,⊥</sup> Naoki Okada,<sup>†</sup> Satoshi Seino,<sup>||</sup> and Shinsaku Nakagawa<sup>\*†,⊥</sup>

Graduate School of Pharmaceutical Sciences and Center for Advanced Medical Engineering and Informatics, Osaka University, 1–6 Yamadaoka, Suita, Osaka 565–0871, Japan, Immunology Frontier Research Center, Osaka University, 1–3 Yamadaoka, Suita, Osaka 565–0871, Japan, Graduate School of Engineering, Osaka University, 2–1 Yamadaoka, Suita, Osaka 565–0871, Japan, and Biomedical MR Science Center, Shiga University of Medical Science, Tsukiwa-cho, Seta, Otsu, Shiga, 520-2192, Japan. Received November 10, 2009; Revised Manuscript Received April 11, 2010

Gold/iron oxide magnetic nanoparticles are hybrid nanoparticles containing a core of magnetic iron oxide and surface colloidal gold, which allows for various biomaterials to be immobilized on the surface of the iron oxide nanoparticles *via* colloidal gold. Here, we developed a novel magnetic resonance (MR) imaging agent to broaden the MR tumor-imaging spectrum of superparamagnetic iron oxide nanoparticles (SPIO), e.g., Feridex, a clinical MR imaging agent for diagnosing liver cancer. Au/Feridex was synthesized by electron beam irradiation, and thiol-modified poly(ethylene glycol) (PEG-SH) was easily conjugated to its surface via an Au–S bond without the need for any chemical reactions. PEG conjugation of Au/Feridex enhanced its accumulation in Meth-A tumor tissue and decreased its accumulation in normal liver tissue. In addition, MRI using PEG-Au/Feridex, in contrast to MRI using unmodified Au/Feridex and Feridex, detected B16BL6 and Meth-A tumor tissues *in vivo*. This finding indicates that PEG-Au/Feridex is useful for diagnosing various types of tumors. In addition, because the synthesis of PEG-Au/Feridex is simple and high yields are easily produced, PEG-modified SPIO for tumor diagnosis can be prepared on an industrial scale with low cost.

### INTRODUCTION

Superparamagnetic iron oxide (SPIO) is a potent contrast agent for magnetic resonance imaging (MRI) (1–4), represented by Feridex (AMAG Pharmaceuticals, Inc., MA) and Resovist (Bayer Schering Pharma AG., Germany). These compounds contain a core iron oxide nanoparticle coated with a dextran polymer. SPIO decreases the signal intensity on T<sub>2</sub> (T<sub>2</sub><sup>\*</sup>)-weighted MR images and is clinically used for diagnosing liver cancer (5–7). SPIO is expected to improve the accuracy and specificity of cancer diagnoses in combination with other diagnostic tools such as computed tomography and ultrasonography (8).

SPIO in the blood is rapidly taken up by the reticular endothelial system (RES) like the hepatic specialized macrophages and Kupffer cells, resulting in a high accumulation in healthy liver tissue (9, 10). On the other hand, SPIO does not accumulate in liver tumor tissue lacking Kupffer cells and does not decrease the signal intensity of tumors, which leads to an

increased contrast between healthy liver tissue and tumor tissue (8–10). Because this mechanism inhibits the distribution of SPIO to other tissues, however, the application of SPIO is limited to the diagnosis of liver cancer. Therefore, many researchers have attempted to develop novel contrast agents for various types of tumors by improving the SPIO (1, 11, 12).

Surface modification of SPIO with various biomaterials to inhibit RES uptake is considered effective for targeting tumors (1). In particular, conjugation with a water-soluble polymer on the SPIO surface is an effective method of inhibiting RES uptake, subsequently prolonging the half-life of SPIO in the blood. A longer blood half-life of SPIO allows for specific accumulation in tumor tissue by an enhanced permeability and retention effect (EPR effect) (1, 13–18). Many methods of surface modification have been reported: encapsulation of SPIO into nanoimmunoliposomes (13), conjugation of SPIO with polymers such as poly(ethylene glycol) (PEG), poly(ethylene oxide), and dextran (17, 19). These approaches, however, require specially designed polymer molecules or complicated preparation methods (20, 21). There is therefore strong interest in developing a simple and easy method of conjugating functional molecules to the SPIO surface.

We developed gold/iron magnetic nanoparticles that are easily synthesized by electron beam irradiation of a mixture of iron oxide nanoparticles and Au solution (22). Using this method, gold/iron magnetic nanoparticles are obtained in extremely high yield (almost 100%). Colloidal gold forms a strong Au–S bond with a thiol group just by mixing, without any catalysts or linker molecules (22–25). This property is useful for conjugating various polymers or biomolecules on the nanoparticle surface. As one application, we previously reported that an adenovirus vector (Ad) could be easily immobilized on the gold/iron nanoparticle via the Au–S bond, allowing the Ad/nanoparticle

\* Corresponding authors. Yohei Mukai, Ph.D., Department of Biotechnology and Therapeutics, Graduate School of Pharmaceutical Sciences, Osaka University, 1–6 Yamadaoka, Suita, Osaka 565–0871, Japan. Tel: +81-6-6879-8178, Fax: +81-6-6879-8179, E-mail: yohe@phs.osaka-u.ac.jp. Shinsaku Nakagawa, Ph.D., Department of Biotechnology and Therapeutics, Graduate School of Pharmaceutical Sciences, Osaka University, 1–6 Yamadaoka, Suita, Osaka 565–0871, Japan. Tel: +81-6-6879-8175, Fax: +81-6-6879-8179, E-mail: nakagawa@phs.osaka-u.ac.jp.

<sup>†</sup> Graduate School of Pharmaceutical Sciences, Osaka University.

<sup>‡</sup> Immunology Frontier Research Center, Osaka University.

<sup>§</sup> Shiga University of Medical Science.

<sup>||</sup> Graduate School of Engineering, Osaka University.

<sup>⊥</sup> Center for Advanced Medical Engineering and Informatics, Osaka University.

complex to be introduced into cells by magnetic force, resulting in great improvement in the gene transduction efficacy of the Ad (23). In the present study, we synthesized a gold/iron magnetic nanoparticle using Feridex, a clinically available SPIO for liver cancer diagnosis, as its core (Au/Feridex). We coated the surface of Au/Feridex using a thiol-modified PEG to inhibit its accumulation in the liver, thereby extending its half-life in the blood, and to target tumors by the EPR effect. We evaluated the efficacy of PEG-conjugated Au/Feridex (PEG-Au/Feridex) as a tumor contrast agent in tumor-bearing mice.

## EXPERIMENTAL PROCEDURES

**Au/Feridex Synthesis.** Feridex (Advanced Magnetics, Inc.) was dispersed at a concentration of 0.1 g/L in an aqueous solution containing 0.5 mM AuHCl<sub>4</sub>, 4.125 mM 2-propanol, and 10 g/L poly(vinyl alcohol) (PVA). The dispersion was poured into a glass vial and irradiated with an electron beam at a dose of 6 kGy. Au/Feridex was purified by high-speed centrifugation and redispersed in distilled water. The size was measured using a dynamic light scattering method with a Z-sizer 3000-HS (Malvern Instruments Ltd., UK).

**Cell Line.** Mouse melanoma cells (B16BL6) were kindly provided from Kobegakuin University. B16BL6 cells were cultured in Minimum Essential Medium (Sigma-Aldrich, St. Louis, MO) containing 7.5% fetal bovine serum (Invitrogen Corporation, Carlsbad, CA) and Antibiotic-Antimycotic Mixed Solution (Nacalai Tesque Inc., Japan). RAW264.7 cells were purchased from American Type Culture Collection. RAW264.7 cells were cultured in Dulbecco's Modified Eagle's Medium (Wako Pure Chemical Industries Ltd., Osaka, Japan) containing 10% fetal bovine serum and Antibiotic-Antimycotic Mixed Solution. Meth-A cells were kindly provided by the Institute of Development, Aging, and Cancer of Tohoku University. Meth-A cells were maintained by intraperitoneal passage in BALB/c mice.

**Transmission Electron Microscopy (TEM) Observation of Feridex and Au/Feridex.** The morphologies of the Feridex and Au/Feridex were observed by a TEM (H-8100T, Hitachi Ltd., Tokyo, Japan) operated at 200 kV. The typical image from several TEM micrographs is shown in this report.

**Preparation of PEG-Conjugated Au/Feridex (PEG-Au/Feridex).** Au/Feridex and thiol-modified PEG (PEG-SH, MW = 5000 Da; NOF Corporation, Japan) were mixed at a ratio of 1:1 (1  $\mu$ mol PEG-SH/mg Fe) in Au/Feridex. The mixture was incubated at room temperature for 1 h and then purified by high-speed centrifugation (28 000 rpm, 30 min). The concentrations of Fe and Au were determined using an inductively coupled plasma (ICP) spectrometer ICPS-7500 (Shimadzu Corporation, Japan).

**PVA Test—Cross-Linking of PEGylated Contrast Agents.** Contrast agents (Feridex or Au/Feridex) and PEGs (PEG-SH or nonmodified PEG, MW = 5000 Da; Wako Pure Chemical Industries Ltd.) were mixed at a ratio of 1:1 (1  $\mu$ mol PEGs/mg Fe). After 1 h incubation at room temperature, the mixtures were purified by high-speed centrifugation (100 000  $\times$  g, 30 min), and the pellet was resuspended with distilled water. An aliquot of 5 mg Fe/mL of these reactants was mixed with an equal volume of 30% PVA (Wako Pure Chemical Industries Ltd.) and incubated at room temperature for 1 h. Cross-linking between PVA and PEG resulted in a precipitate that contained the nanoparticles (26).

**Quantification of PEG-SH Immobilized on Contrast Agents.** Feridex and Au/Feridex were mixed with PEG-SH at a ratio of 1:1 (1  $\mu$ mol PEGs/mg Fe). After 1 h incubation at room temperature, the mixtures were purified by high-speed centrifugation (100 000  $\times$  g, 30 min). The amount of sulfur

contained in PEG-SH in each sample was then determined using an ICP spectrometer.

**In Vitro MRI.** Feridex, Au/Feridex, and PEG-Au/Feridex were diluted with distilled water to contain the same iron concentration (50  $\mu$ g/mL, 10  $\mu$ g/mL, and 2  $\mu$ g/mL). T<sub>2</sub>-weighted images (multislice spin-echo coronal images; TR = 2000 ms, TE = 69 ms) of these solutions were obtained with a 1.5 T MRI (MRminiSA; DS Pharma Biomedical Co., Ltd., Japan).

**In Vivo Blood Clearance.** BALB/c mice were intravenously injected with 1 mg Fe in contrast agents (Feridex, Au/Feridex, and PEG-Au/Feridex). Blood samples were collected at 2, 5, 10, 30, and 60 min postinjection. T<sub>2</sub>-weighted images of these samples were obtained with a 1.5 T MRI (MRminiSA; DS Pharma Biomedical Co., Ltd., Japan). The signal intensity of each sample on the MR image was analyzed using *Image J* software (National Institutes of Health, USA). The iron concentration of the samples was calculated based on the correlation between the signal intensity and the iron concentration of Feridex. All studies involving animals were approved by the institute's animal care and use committee.

**In Vivo Distribution.** Meth-A cells ( $5 \times 10^5$  cells/100  $\mu$ L) were injected intradermally into the abdomen of 6-week-old BALB/c mice. When the tumor size reached 10 mm in diameter, 1 mg Fe/200  $\mu$ L of each contrast agent (Au/Feridex, PEG-Au/Feridex) was injected intravenously into the mice ( $n = 3$  mice per group). The mice were killed, and the tumor and liver were extracted at 1 or 24 h postinjection and immediately freeze-dried. Radiation was counted after irradiation of vials containing samples in a nuclear reactor (JRR-3 in Japan Atomic Energy Agency, Ibaragi, Japan) with a thermal neutron flux of  $5.2 \times 10^{17}$  neutrons/cm<sup>2</sup>s for 20 min. After a delay of 4 to 5 days, irradiated samples were counted by computer-based  $\gamma$ -ray spectrometry on a Ge detector for 2000 s, and then the peak area of 412 keV  $\gamma$ -rays from <sup>198</sup>Au elements was measured using a multichannel pulse height analyzer with automatic dead time (<10%) correction.

**In Vivo MR Tumor Imaging.** C57BL/6 mice (6 weeks old) were injected intradermally in the abdomen with  $5 \times 10^5$  cells/100  $\mu$ L of B16BL6 cells. Meth-A tumor-bearing mice were prepared as described below. When the tumors were 10 mm in diameter, 1 mg Fe/200  $\mu$ L of each contrast agent (Feridex, Au/Feridex, PEG-Au/Feridex) was injected into the mice ( $n = 3$  mice per group). MRI studies were performed with MRminiSA (DS Pharma Biomedical Co., Ltd.). Tumor-bearing mice were anesthetized with a 1.5% isoflurane/air mixture and maintained at 37 °C inside the magnet. All images were obtained as T<sub>2</sub>-weighted images (multislice spin-echo axial images; TR = 2000 ms, TE = 69 ms). MRI scans were performed before and 1 h after the injection.

**Iron Staining of Tumor Sections.** After *in vivo* MRI analysis, the tumor and liver were extracted and fixed with 4% paraformaldehyde followed by sequential immersion in 10%, 20%, and 30% sucrose solutions. Tissues were frozen in OCT compound (Sakura Finetek Inc., Torrance, CA) with liquid nitrogen and sectioned at 10  $\mu$ m using a cryostat (CM1850; Leica Microsystems GmbH). Sections were stained with Prussian blue to detect the particles of Feridex, Au/Feridex, and PEG-Au/Feridex. Sections were stained with 1% potassium hexacyanoferrate (II)-trihydrate in 0.1 M HCl followed by counterstaining with 0.5% eosin Y ethanol solution.

## RESULTS

**Synthesis of PEG-Au/Feridex.** Au/Feridex was synthesized by electron beam irradiation of the mixture of AuHCl<sub>4</sub> and the Feridex solution. Synthesis of Au/Feridex was confirmed by transmission electron microscopy (Figure 1). Au/Feridex was visualized as colloidal gold nanoparticles (black particles) on

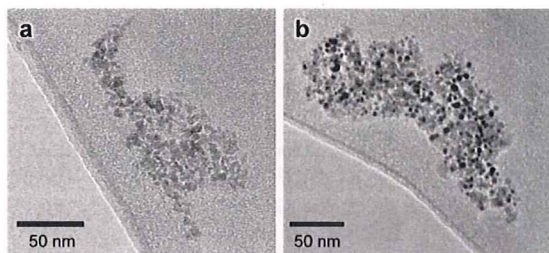


**Figure 1.** Transmission electron microscopy image of (a) Feridex and (b) Au/Feridex.

the surface of Feridex (gray particles; Figure 1b). Unreacted Feridex, i.e., without colloidal gold, was not observed in this solution. The ratio of Au/Fe was determined as 0.944 Au/Fe by weight using an ICP spectrometer.

PEG conjugation of Au/Feridex was performed by mixing PEG-SH (MW = 5000 Da) with Au/Feridex. PEG conjugation was confirmed by a PVA test, in which PEG-modified particles form a precipitate due to hydrogen bonding between PEG and PVA (26). Precipitation was observed only in the PEG-SH and Au/Feridex mixture, and there was no precipitate in the other mixtures (PEG-SH and Feridex, PEG and Au/Feridex, Au/Feridex alone; Figure 2). This finding indicated that PEG modification of Feridex was achieved by an Au–S bond.

**Characterization of PEG–Au/Feridex.** We measured the amount of PEG-SH immobilized on Au/Feridex using an ICP spectrometer. The amount of immobilized PEG-SH on Au/Feridex was 1.58 mg PEG-SH/mg Fe (1.74 mg PEG-SH/mg Au) and the amount immobilized on Feridex was 0.038 mg. This finding also suggests that PEG-SH was efficiently immobilized on Au/Feridex via Au–S bonds.

We measured the hydrodynamic size of these contrast agents (Feridex, Au/Feridex, and PEG–Au/Feridex) using a dynamic light scattering method. The hydrodynamic size of Feridex, Au/Feridex, and PEG–Au/Feridex was 69.4 nm, 163.9 nm, and 153.6 nm, respectively. Notably, the size of PEG–Au/Feridex (153.6 nm) was smaller than that of Au/Feridex (163.9 nm), suggesting that the state of dispersion was improved by PEG conjugation. The state of dispersion is an important factor in tumor targeting using the EPR effect (27, 28). Therefore, this result suggests that PEG–Au/Feridex may be able to effectively target tumors. PEG–Au/Feridex was not cytotoxic to RAW264.7 cells at a concentration of 300  $\mu\text{g Fe/mL}$  (Supporting Information Figure S1). In fetal bovine serum at 37 °C, the Au–S bond remained unbroken after 1 h incubation (Supporting Information Figure S2). Moreover, PEG–Au/Feridex did not aggregate under this condition (data not shown). These results suggested that this

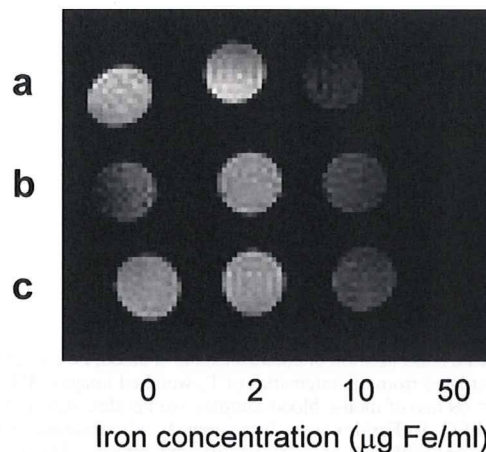


**Figure 3.**  $T_2$ -weighted images of each contrast agent. (a) Feridex, (b) Au/Feridex, and (c) PEG–Au/Feridex were diluted to the same iron concentration with distilled water.  $T_2$ -weighted images (spin-echo sequence; TR = 2000 ms, TE = 69 ms) were obtained using MRminiSA.

conjugation method using the Au–S bond is suitable for *in vivo* applications.

We then evaluated the transverse  $T_2$  relaxation time of the three contrast agents using *in vitro* MRI images. All the contrast agents showed relaxation at an iron concentration of 10  $\mu\text{g/mL}$  (Figure 3). These results indicate that the  $T_2$  relaxation time was maintained after modification of colloidal gold and PEG-SH, suggesting that PEG–Au/Feridex and Feridex, a clinically used contrast agent, have a nearly equal  $T_2$  relaxation.

**Distribution of Each Contrast Agent.** The efficacy of PEG modification was estimated by analyzing the blood clearance of Feridex, Au/Feridex, and PEG–Au/Feridex. Blood concentrations of each contrast agent were measured after intravenous injection into mice. The initial Fe concentration in the blood of mice injected with PEG–Au/Feridex was higher than in mice injected with Feridex and Au/Feridex (Figure 4). In addition, the clearance of PEG–Au/Feridex was moderate compared with that of Feridex and Au/Feridex (Figure 4). These findings suggest that the blood concentration of the imaging agent is increased by PEG modification.

We then evaluated the accumulation of the contrast agent in the liver and tumor. Au/Feridex and PEG–Au/Feridex were intravenously injected into Meth-A tumor-bearing BALB/c mice. At 1 h postinjection, the distribution in the liver and tumor tissues was determined by radiochemical neutron

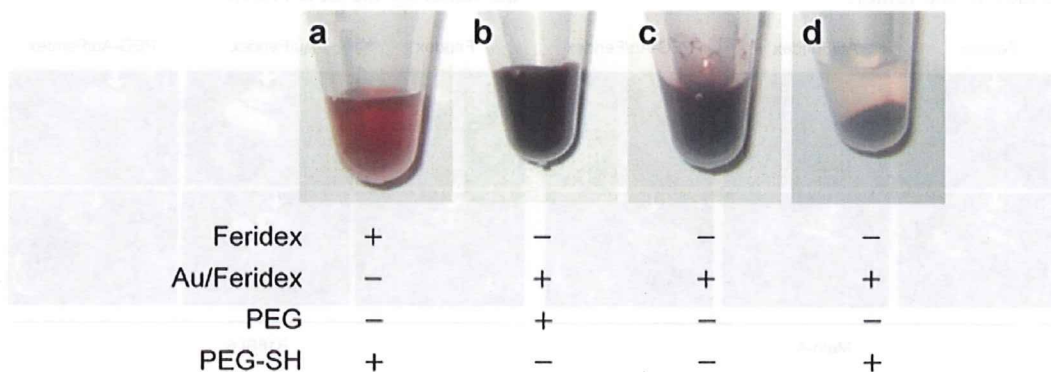


**Figure 2.** Confirmation of PEG-conjugation to Au/Feridex. PEGs (nonmodified PEG and thiol-modified PEG) were mixed with 5 mg Fe/mL of contrast agents (Feridex and Au/Feridex), as shown in the figure, and purified by high-speed centrifugation. The purified mixtures were mixed with PVA to a final concentration of 15% PVA and incubated overnight at room temperature.

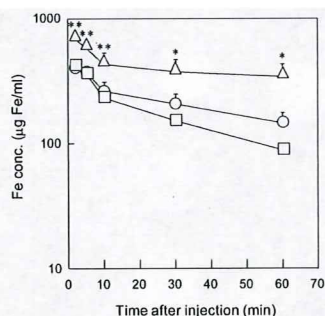


**Figure 4.** Fe concentration of contrast agents in blood. Fe concentrations were calculated from the intensities of T<sub>2</sub>-weighted images (TR = 2000 ms, TE = 69 ms) of mouse blood samples. (○) Feridex, (□) Au/Feridex, and (△) PEG-Au/Feridex were intravenously administered and blood samples were collected at 2, 5, 10, 30, and 60 min. The error bars represent the SEM ( $n = 5$ ). \* $P < 0.001$ , \*\* $P < 0.0001$  by two-tailed  $t$ -test.

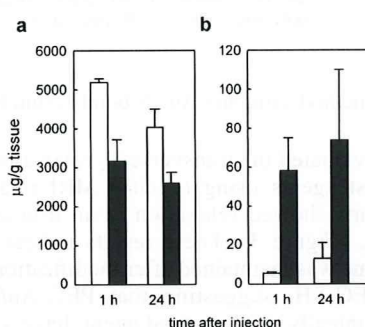


**Figure 5.** Accumulation of contrast agents in the liver and tumor. Au/Feridex and PEG-Au/Feridex were intravenously injected into tumor-bearing mice, and the livers and tumors were extracted 1 h postinjection. The quantity of (□) Au/Feridex and (■) PEG-Au/Feridex accumulated in the (a) liver or (b) tumor was measured by radiochemical neutron activation analysis of the Au element. Each bar represents SEM ( $n = 3$ ).

activation analysis of the Au element (Figure 5). Liver accumulation of Au/Feridex was decreased by PEG conjugation (Figure 5a), suggesting that PEG conjugation inhibited uptake of the SPIO by the Kupffer cells in the liver. In the tumor, the accumulation of PEG-Au/Feridex was approximately 10-fold higher than that of Au/Feridex (Figure 5b). Accumulation of PEG-Au/Feridex in the tumor at 24 h was slightly increased compared with that at 1 h. The findings suggest that PEG conjugation efficiently enhanced the targeting of Feridex to the tumor.

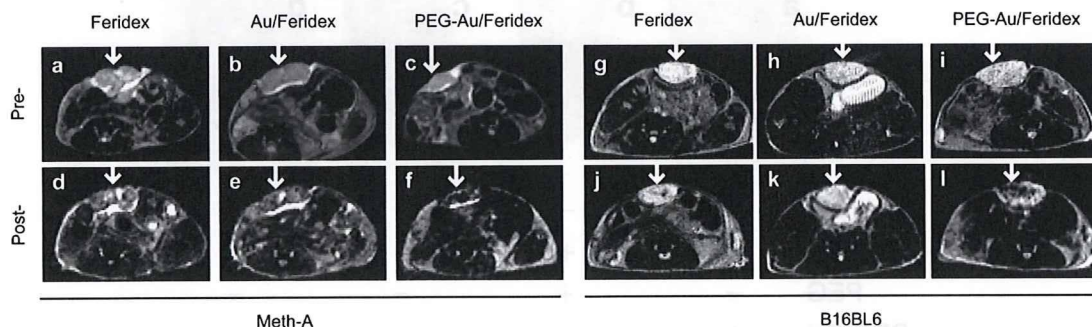


**Figure 6.** In vivo MRI tumor imaging. T<sub>2</sub>-weighted images (1.5 T, spin-echo sequence: TR = 2000 ms, TE = 69 ms) of tumor-bearing mice (a–f, Meth-A; g–l, B16BL6) taken pre- and 1 h postinjection of 1 mg Fe of contrast agent (a,d,g,j: Feridex; b,e,h,k: Au/Feridex; c,f,i,l: PEG-Au/Feridex). Images a–c and g–i were obtained preinjection, and images d–f and j–l were obtained 1 h postinjection. Arrowhead indicates tumor. All images were obtained using MRminiSA.

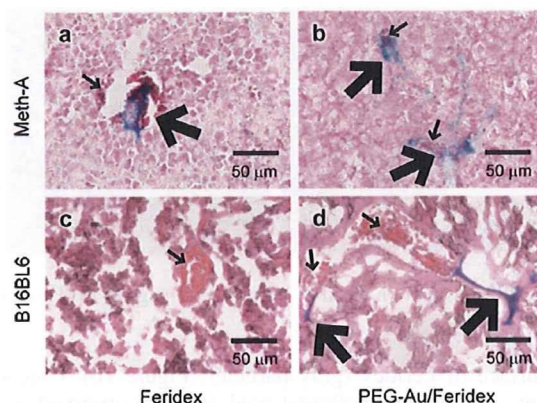


**Figure 7.** Analysis of tumor-accumulating mechanism of PEG-Au/Feridex. Ex vivo Prussian blue-stained images of tumor tissues extracted from tumor-bearing mice (a,b: Meth-A; c,d: B16BL6) at 1 h postinjection of 1 mg Fe of (a,c) Feridex or (b,d) PEG-Au/Feridex (counterstaining: eosin staining). Narrow arrowhead indicates tumor blood vessel in which erythrocytes are observed. Bold arrowhead indicates location of contrast agents.

**PEG-Au/Feridex Enhances Tumor Contrast by an EPR Effect in MR Imaging.** We used MR imaging to visualize the efficacy of PEG-conjugated Au/Feridex. MRI of Meth-A tumor-bearing mice was performed 1 h postinjection of Feridex, Au/Feridex, and PEG-Au/Feridex. T<sub>2</sub>-weighted images showed that PEG-Au/Feridex decreased the signal intensity of the tumor, leading to the clear identification of a Meth-A tumor, whereas Feridex and Au/Feridex did not improve the tumor contrast (Figure 6a–f). Similar results were obtained using B16BL6 melanoma bearing mice (Figure 6g–l). These results suggested that our PEG-Au/Feridex was effective for identifying various tumor types.

We also tried to determine the mechanism of accumulation in the tumor by analyzing the location of these contrast agents in the tumor tissue. Tumor tissues were extracted from the same mice used to take the MR images, and then slices of the tissues were stained using the Prussian blue staining method to detect the Fe molecules. In both Meth-A and B16BL6-injected mice, PEG-Au/Feridex was distributed around the tumor blood vessels (Figure 7), suggesting that PEG-Au/Feridex leaked from the tumor blood vessels to the outside through the leaky tumor vascular walls. On the other hand, Feridex was not detected in the tumor sections (Figure 6). These results suggest that PEG-Au/Feridex has a decreased liver uptake and accumulated in the tumor by the EPR effect.

## DISCUSSION

Several studies have been performed in an effort to develop tumor-targeted SPIO (1). Most of the previously developed methods, however, require polymers containing special functional groups and some reaction steps that complicate the synthesis of surface-modified SPIO. Moreover, the low yield at each step of the reaction limits the usefulness (19). In the present study, these problems were overcome by the use of our original nanomaterial, an Au/Fe magnetic nanoparticle. We designed Au/Feridex from Feridex, a clinically used SPIO coated with dextran. Au immobilization on Feridex was achieved simply (an electron beam irradiation) and its efficiency was almost 100% based on TEM observation (Figure 1). This Au immobilization method is also successful for other iron oxide nanoparticles that do not contain surface dextran (23), suggesting that this technology is applicable to various types of SPIO. PEG conjugation via Au-S bonds proceeded under mild conditions at room temperature, without any catalysts or special chemical reactions. The number of PEG-SH molecules on PEG-Au/Feridex was estimated to be approximately 3000 molecules/particle (100 molecules/colloidal gold) based on the assumption that Au/Feridex is a 150-nm-diameter sphere and colloidal gold is a 3.4-nm diameter sphere, which was supported by TEM images (Figure 1). Moreover, the efficiency of PEG conjugation was also estimated to be almost 100%, supported by the clear supernatant in the PVA test (Figure 2). Therefore, this conjugation method is simpler, easier, and more efficient than previously described methods (13, 14, 16–19, 29). In this aspect, Au/Fe magnetic nanoparticles are an innovative tool that retains the activity of the conjugated molecules (23). The efficacy of PEG conjugation was demonstrated by the pharmacokinetics (Figure 4). The higher Fe concentration of PEG-Au/Feridex in the early phase suggests that the distribution volume was decreased and indicates that PEG conjugation inhibited uptake of Au/Feridex into liver (Figure 5). These results clearly show that Au immobilization and surface modification of SPIO is useful for creating a novel MRI tumor contrast agent.

On the other hand, the size of the PEG-conjugated contrast agents is important for tumor targeting (27). The size of the gold/iron magnetic nanoparticles can be easily altered by changing the core particle size (23). This feature might allow for better control of the pharmacokinetics of the contrast agent (15, 27). An effective tumor-targeting method may thus be developed by controlling two parameters: the particle size and the targeting agent. In the future, innovative methods to target various diseases may be developed by synthesizing smaller gold/iron magnetic nanoparticles to decrease the accumulation in the liver, and by applying various targeting agents to control the pharmacokinetics. Our novel MRI contrast agents have high potential for the diagnosis of various diseases.

## CONCLUSION

The present paper reports a novel MRI tumor contrast agent (PEG-Au/Feridex) produced using a unique technique. Here, we showed that Au/Feridex can be simply and easily conjugated with PEG-SH. At each reaction step (synthesis of Au/Feridex and modification with PEG-SH), the yield was approximately 100%. PEG-Au/Feridex uptake was decreased in the liver and its accumulation in the tumor was approximately 10-fold greater than that of Au/Feridex, which led to clear identification of the tumor on T<sub>2</sub>-weighted images that could not be achieved with Feridex alone. This newly developed contrast agent can be modified with various targeting agents containing a thiol group and will thus be potentially very useful for the diagnosis of various diseases.

## ACKNOWLEDGMENT

This study was supported by Research for Promoting Technological Seeds from the Japan Science and Technology Agency (JST); in part by a Grant-in-Aid for Scientific Research and a Grant-in-Aid for Young Scientists (B) from the Ministry of Education, Culture, Sports, Science, and Technology of Japan (MEXT) and the Japan Society for the Promotion of Science (JSPS); in part by a Research Fund Project on Health Sciences focusing on Drug Innovation from the Japan Health Sciences Foundation; and in part by the Magnetic Health Science Foundation. Feridex was kindly provided by Eiken Chemical Co. Ltd. (Tokyo, Japan). Radiochemical neutron activity analysis of the Au element was performed by Dr. Norio Ito at the Osaka Prefecture University (Osaka, Japan).

**Supporting Information Available:** Additional figures as described in the text. This material is available free of charge via the Internet at <http://pubs.acs.org>.

## LITERATURE CITED

- (1) Corot, C., Robert, P., Idee, J. M., and Port, M. (2006) Recent advances in iron oxide nanocrystal technology for medical imaging. *Adv. Drug Delivery Rev.* 58, 1471–1504.
- (2) Ferrucci, J. T., and Stark, D. D. (1990) Iron oxide-enhanced MR imaging of the liver and spleen: review of the first 5 years. *Am. J. Roentgenol.* 155, 943–950.
- (3) de Vries, I. J., Lesterhuis, W. J., Barentsz, J. O., Verdijk, P., van Krieken, J. H., Boerman, O. C., Oyen, W. J., Bonenkamp, J. J., Boezeman, J. B., Adema, G. J., Bulte, J. W., Scheenen, T. W., Punt, C. J., Heerschap, A., and Figdor, C. G. (2005) Magnetic resonance tracking of dendritic cells in melanoma patients for monitoring of cellular therapy. *Nat. Biotechnol.* 23, 1407–1413.
- (4) Bulte, J. W., and Kraitchman, D. L. (2004) Iron oxide MR contrast agents for molecular and cellular imaging. *NMR Biomed.* 17, 484–499.
- (5) Kopp, A. F., Laniado, M., Dammann, F., Stern, W., Gronewaller, E., Balzer, T., Schimpfky, C., and Claussen, C. D. (1997) MR imaging of the liver with Resovist: safety, efficacy, and pharmacodynamic properties. *Radiology* 204, 749–756.
- (6) Reimer, P., and Tombach, B. (1998) Hepatic MRI with SPIO: detection and characterization of focal liver lesions. *Eur. Radiol.* 8, 1198–1204.
- (7) Hahn, P. F., Stark, D. D., and Ferrucci, J. T. (1992) Accumulation of iron oxide particles around liver metastases during MR imaging. *Gastrointest. Radiol.* 17, 173–174.
- (8) Tanimoto, A., and Kuribayashi, S. (2006) Application of superparamagnetic iron oxide to imaging of hepatocellular carcinoma. *Eur. J. Radiol.* 58, 200–216.
- (9) Raynal, I., Prigent, P., Peyramaure, S., Najid, A., Rebutzi, C., and Corot, C. (2004) Macrophage endocytosis of superparamagnetic iron oxide nanoparticles: mechanisms and comparison of ferumoxides and ferumoxtran-10. *Invest. Radiol.* 39, 56–63.
- (10) Rogers, W. J., and Basu, P. (2005) Factors regulating macrophage endocytosis of nanoparticles: implications for targeted magnetic resonance plaque imaging. *Atherosclerosis* 178, 67–73.
- (11) Peng, X. H., Qian, X., Mao, H., Wang, A. Y., Chen, Z. G., Nie, S., and Shin, D. M. (2008) Targeted magnetic iron oxide nanoparticles for tumor imaging and therapy. *Int. J. Nanomed.* 3, 311–321.
- (12) Liu, S., Jia, B., Qiao, R., Yang, Z., Yu, Z., Liu, Z., Liu, K., Shi, J., Ouyang, H., Wang, F., and Gao, M. (2009) A novel type of dual-modality molecular probe for MR and nuclear imaging of tumor: preparation, characterization and in vivo application. *Mol. Pharmacol.* 6, 1074–1082.

- (13) Yang, C., Rait, A., Pirollo, K. F., Dagata, J. A., Farkas, N., and Chang, E. H. (2008) Nanoimmunoliposome delivery of superparamagnetic iron oxide markedly enhances targeting and uptake in human cancer cells in vitro and in vivo. *Nanomedicine* 4, 318–329.
- (14) Kumagai, M., Imai, Y., Nakamura, T., Yamasaki, Y., Sekino, M., Ueno, S., Hanaoka, K., Kikuchi, K., Nagano, T., Kaneko, E., Shimokado, K., and Kataoka, K. (2007) Iron hydroxide nanoparticles coated with poly(ethylene glycol)-poly(aspartic acid) block copolymer as novel magnetic resonance contrast agents for in vivo cancer imaging. *Colloids Surf., B: Biointerfaces* 56, 174–181.
- (15) Larsen, E. K., Nielsen, T., Wittenborn, T., Birkedal, H., Vorup-Jensen, T., Jakobsen, M. H., Ostergaard, L., Horsman, M. R., Besenbacher, F., Howard, K. A., and Kjems, J. (2009) Size-dependent accumulation of PEGylated silane-coated magnetic iron oxide nanoparticles in murine tumors. *ACS Nano* 3, 1947–1951.
- (16) Lee, H., Lee, E., Kim do, K., Jang, N. K., Jeong, Y. Y., and Jon, S. (2006) Antibiofouling polymer-coated superparamagnetic iron oxide nanoparticles as potential magnetic resonance contrast agents for in vivo cancer imaging. *J. Am. Chem. Soc.* 128, 7383–7389.
- (17) Zhang, Y., Kohler, N., and Zhang, M. (2002) Surface modification of superparamagnetic magnetite nanoparticles and their intracellular uptake. *Biomaterials* 23, 1553–1561.
- (18) Chen, T. J., Cheng, T. H., Hung, Y. C., Lin, K. T., Liu, G. C., and Wang, Y. M. (2008) Targeted folic acid-PEG nanoparticles for noninvasive imaging of folate receptor by MRI. *J. Biomed. Mater. Res., Part A* 87, 165–175.
- (19) Thunemann, A. F., Schutt, D., Kaufner, L., Pison, U., and Mohwald, H. (2006) Maghemite nanoparticles protectively coated with poly(ethylene imine) and poly(ethylene oxide)-block-poly(glutamic acid). *Langmuir* 22, 2351–2357.
- (20) Moghimi, S. M., Hunter, A. C., and Murray, J. C. (2001) Long-circulating and target-specific nanoparticles: theory to practice. *Pharmacol. Rev.* 53, 283–318.
- (21) Beduneau, A., Ma, Z., Grotelas, C. B., Kabanov, A., Rabinow, B. E., Gong, N., Mosley, R. L., Dou, H., Boska, M. D., and Gendelman, H. E. (2009) Facilitated monocyte-macrophage uptake and tissue distribution of superparamagnetic iron-oxide nanoparticles. *PLoS One* 4, e4343.
- (22) Mizukoshi, Y., Seino, S., Okitsu, K., Kinoshita, T., Otome, Y., Nakagawa, T., and Yamamoto, T. A. (2005) Sonochemical preparation of composite nanoparticles of Au/gamma-Fe<sub>2</sub>O<sub>3</sub> and magnetic separation of glutathione. *Ultrason. Sonochem.* 12, 191–195.
- (23) Kamei, K., Mukai, Y., Kojima, H., Yoshikawa, T., Yoshikawa, M., Kiyohara, G., Yamamoto, T. A., Yoshioka, Y., Okada, N., Seino, S., and Nakagawa, S. (2009) Direct cell entry of gold/iron-oxide magnetic nanoparticles in adenovirus mediated gene delivery. *Biomaterials* 30, 1809–1814.
- (24) Seino, S., Otome, T., Maki, Y., Nakagawa, T., Okitsu, T., Mizukoshi, K., Nakayama, Y., Sekino, T., Niihara, T., and Yamamoto, T. A. (2004) Gamma-ray synthesis of composite nanoparticles of noble metals and magnetic iron oxides. *Scr. Mater.* 51, 467–472.
- (25) Seino, S., Nakagawa, T., Kojima, T., Taniguchi, T., Okuda, R., and Yamamoto, T. A. (2007) Radiation induced synthesis of gold/iron-oxide composite nanoparticles using high-energy electron beam. *J. Nanopart. Res.* 10, 1071–1076.
- (26) Fujita, M. (2006) Patent No. JP 2006–327962A.
- (27) Pouliquen, D., Le Jeune, J. J., Perdrisot, R., Ermias, A., and Jallet, P. (1991) Iron oxide nanoparticles for use as an MRI contrast agent: pharmacokinetics and metabolism. *Magn. Reson. Imaging* 9, 275–283.
- (28) van Vlerken, L. E., Vyas, T. K., and Amiji, M. M. (2007) Poly(ethylene glycol)-modified nanocarriers for tumor-targeted and intracellular delivery. *Pharm. Res.* 24, 1405–1414.
- (29) Larsen, E. K., Nielsen, T., Wittenborn, T., Birkedal, H., Vorup-Jensen, T., Jakobsen, M. H., Ostergaard, L., Horsman, M. R., Besenbacher, F., Howard, K. A., and Kjems, J. (2009) Size-dependent accumulation of PEGylated silane-coated magnetic iron oxide nanoparticles in murine tumors. *ACS Nano* 3, 1947–1951.

BC900487P

Preparation for Highly Sensitive MRI Contrast Agents Using  
Core/Shell Type Nanoparticles Consisting of Multiple SPIO Cores  
with Thin Silica CoatingKazuo Tanaka,<sup>†</sup> Asako Narita,<sup>†</sup> Narufumi Kitamura,<sup>†</sup> Wataru Uchiyama,<sup>†</sup> Masahito Morita,<sup>‡,§</sup>  
Toshiro Inubushi,<sup>§</sup> and Yoshiki Chujo<sup>\*,†</sup><sup>†</sup>Department of Polymer Chemistry, Graduate School of Engineering, Kyoto University, Katsura, Nishikyo-ku,  
Kyoto 615-8510, Japan, <sup>‡</sup>WPI Immunology Frontier Research Center, Osaka University, Suita,  
Osaka 565-0871, Japan, and <sup>§</sup>Biomedical MR Science Center, Shiga University of Medical Science,  
Seta Tsukinowa-cho, Otsu 520-2192, Japan

Received April 16, 2010. Revised Manuscript Received May 13, 2010

We describe here the facile and robust preparation methods for the multiple-SPIO-containing silica-coated core/shell type nanoparticles which can serve as a highly sensitive MRI contrast agent. The imidazolium-tethered core/shell type particles were synthesized, and the centrifugal selection for the multiple-SPIO-containing particles and the etching process to fabricate thin silica layers were carried out to improve the proton relaxivity of water tissue. We found that the synthetic particles can provide ~7-fold clearer contrasts than that of the particles before treatments. In addition, the particles can show good dispersibility at least for 1 week in aqueous media.

## Introduction

Magnetic resonance imaging (MRI) is one of the powerful diagnostic tools in modern clinical medicine, and contrast agents can improve sensitivity and specificity in the detection. Superparamagnetic iron oxide (SPIO) particles can accelerate the proton transverse relaxation of water tissue in aqueous media and consequently provide hypointense (dark) contrast in magnetic resonance images on  $T_2$ - and  $T_2^*$ -weighted sequences.<sup>1</sup> Various advanced techniques using SPIO particles such as the cell labeling,<sup>2</sup> biosensors,<sup>3</sup> and in vivo imaging<sup>4</sup> with MRI have been developed. Thus, the SPIO-based contrast agents can be a suitable platform for the advanced imaging probes. However, the improvement of the sensitivity of contrast agents has still remained as a critical issue to ensure the accuracy in the detection and reduce burdens in loaded organisms.

The naked SPIO particles are extremely reactive, and aggregation or nonspecific adsorption with proteins or other substances

would spoil the sensitivity under biological conditions. Therefore, the surface modifications of SPIO particles, for example, with dextran and organic or inorganic polymers, are necessary to maintain dispersion state and prevent from signal loss.<sup>1b,5</sup> The silica-coated core/shell type particles are one of potential platforms for multifunctional molecular probes.<sup>6</sup> The size, shape, and the surface modification which dominate the characteristics, distribution, and toxicity of the particles can be readily tuned.<sup>7</sup> We have reported the preparation method of the MRI contrast agents based on the silica-coated core/shell type SPIO particles which can show good biocompatibility in the mice.<sup>8</sup> However, the sensitivity in MRI was inevitably reduced by the silica coating on the surfaces. The regulation of the thickness of the shell in the core/shell type particles as well as the maximizing the SPIO core content should be still critical issue to overcome the trade-off relationship between the sensitivity and stability of the particles.

Herein, we report the facile method for improving the sensitivity of the core/shell type silica-coated SPIO as MRI contrast agents. Initially, the multiple SPIO particles were accumulated and immobilized into the nanoparticles covered with the silica shell. After the centrifugal separation, the core/shell particles which include multiple SPIO-cores were isolated. Subsequently to minimize the shell thickness, the etching under the alkaline condition was executed, and the multiple SPIO-containing core/shell type nanoparticles with thin silica shell were obtained. Finally,

\*Corresponding author: e-mail [chujoy@chujoy.synchem.kyoto-u.ac.jp](mailto:chujoy@chujoy.synchem.kyoto-u.ac.jp); Fax +81-75-383-2605; Ph +81-75-383-2604.

(1) (a) Laurent, S.; Forge, D.; Port, M.; Roch, A.; Robic, C.; Vander Elst, L.; Muller, R. N. *Chem. Rev.* **2008**, *108*, 2064–2110. (b) Na, H. B.; Song, I. C.; Hyeon, T. *Adv. Mater.* **2009**, *21*, 2133–2148. (c) Gupta, A. K.; Gupta, M. *Biomaterials* **2005**, *26*, 3995–4021. (d) Jeong, U.; Teng, X.; Wang, Y.; Yang, H.; Xia, Y. *Adv. Mater.* **2007**, *19*, 33–60.

(2) (a) Bulte, J. W. M.; Kraitchman, D. L. *NMR Biomed.* **2004**, *17*, 484–499. (b) Arbab, A. S.; Bashaw, L. A.; Miller, B. R.; Jordan, E. K.; Bulte, J. W. M.; Frank, J. A. *Transplantation* **2003**, *76*, 1123–1130. (c) Corot, C.; Robert, P.; Idee, J.-M.; Port, M. *Adv. Drug Delivery Rev.* **2006**, *58*, 1471–1504. (d) Frank, J. A.; Miller, B. R.; Arbab, A. S.; Zywicke, H. A.; Jordan, E. K.; Lewis, B. K.; Bryant, L. H., Jr.; Bulte, J. W. M. *Radiology* **2003**, *228*, 480–487. (e) Wilhelm, C.; Gazeau, F. *Biomaterials* **2008**, *29*, 3161–3174.

(3) (a) Katz, E.; Willner, I. *Angew. Chem., Int. Ed.* **2004**, *43*, 6042–6108. (b) Perez, J. M.; Josephson, L.; Weissleder, R. *ChemBioChem* **2004**, *5*, 261–264. (c) Yigit, M. V.; Mazumdar, D.; Kim, H.-K.; Lee, J. H.; Odintsov, B.; Lu, Y. *ChemBioChem* **2007**, *8*, 1675–1678. (d) Tanaka, K.; Kitamura, N.; Morita, M.; Inubushi, T.; Chujo, Y. *Bioorg. Med. Chem. Lett.* **2008**, *18*, 5463–5465. (e) Atanasijevic, T.; Jasanoff, A. *Nature Protoc.* **2007**, *2*, 2582–2589.

(4) (a) Medarova, Z.; Pham, W.; Farrar, C.; Petkova, V.; Moore, A. *Nature Med.* (N. Y., N.Y. U. S.) **2007**, *13*, 372–377. (b) Lewin, M.; Carlesso, N.; Tung, C.-H.; Tang, X.-W.; Cory, D.; Scadden, D. T.; Weissleder, R. *Nature Biotechnol.* **2000**, *18*, 410–414. (c) Sun, C.; Lee, J. S. H.; Zhang, M. *Adv. Drug Delivery Rev.* **2008**, *60*, 1252–1265. (d) Huh, Y.-M.; Jun, Y.-W.; Song, H.-E.; Kim, S.; Choi, J.-S.; Lee, J.-H.; Yoon, S.; Kim, K.-S.; Shin, J.-S.; Shu, J.-S.; Cheon, J. J. *Am. Chem. Soc.* **2005**, *127*, 12387–12391.

(5) (a) Mornet, S.; Vasseur, S.; Grasset, F.; Duguet, E. *J. Mater. Chem.* **2004**, *14*, 2161–2175. (b) Storm, G.; Blliot, S. O.; Daemen, T.; Lasic, D. D. *Adv. Drug Delivery Rev.* **1995**, *17*, 31–48.

(6) (a) Graf, C.; Vossen, D. L. J.; Imhof, A.; van Blaaderen, A. *Langmuir* **2003**, *19*, 6693–6700. (b) Liz-Marzán, L. M.; Giersig, M.; Mulvaney, P. *Langmuir* **1996**, *12*, 4329–4335. (c) Burns, A.; Ow, H.; Wiesner, U. *Chem. Soc. Rev.* **2006**, *35*, 1028–1042.

(7) (a) Matsumure, Y.; Maeda, H. *Cancer Res.* **1986**, *46*, 6387–6392. (b) Oberdörster, G.; Oberdörster, E.; Oberdörster, J. *Environ. Health Perspect.* **2005**, *113*, 823–839. (c) Auffan, M.; Rose, J.; Bottero, J.-Y.; Lowry, G. V.; Jolivet, J.-P.; Wiesner, M. R. *Nature Nanotechnol.* **2009**, *4*, 634–641. (d) Nishimori, H.; Kondoh, M.; Isoda, K.; Tsunoda, S.; Tsutsumi, Y.; Yagi, K. *Eur. J. Pharm. Biopharm.* **2009**, *72*, 496–501.

(8) Naka, K.; Narita, A.; Tanaka, Y.; Chujo, Y.; Morita, M.; Inubushi, T.; Nishimura, I.; Hiruta, J.; Shibayama, H.; Koga, M.; Ishibashi, S.; Seki, J.; Kizaka-Kondoh, S.; Hiraoka, M. *Polym. Adv. Technol.* **2008**, *19*, 1241–1249.

it was confirmed from the evaluation of the relaxivity of the synthetic particles as a MRI contrast agent that the sensitivity of the resulting SPIO can be improved by 8-fold by our method.

### Experimental Section

**General.**  $^1\text{H}$  NMR spectra were obtained with a JEOL EX-400 spectrometer (400 MHz). Transmission electron microscopy (TEM) measurements were performed using a JEOL JEM-100SX operated at 100 kV electron beam accelerating voltage. One drop of the sample solution was deposited onto a copper grid, and the excess of the droplet was blotted off the grids with filter paper; then the sample was dried under ambient conditions. FT-IR spectra were recorded on a Perkin-Elmer 1600 infrared spectrophotometer using a KBr disk dispersed with the powdered sample. UV-vis absorption spectra were obtained with a Shimadzu UV-3600 UV-vis-NIR spectrophotometer.

**Materials.** Iron(III) chloride hexahydrate, iron(II) chloride tetrahydrate, 28% aqueous ammonium hydroxylate solution, and oleic acid were purchased from Wako Pure Chemical Industries, Ltd. 1-Methylimidazole, 3-chloropropyltriethoxysilane, and Igepal CO-520 were purchased from Aldrich Chemical Co. Tetraethoxysilane was purchased from Tokyo Chemical Industry Co., Ltd. 1-Methylimidazole was dried and distilled under reduced pressure over sodium in a nitrogen atmosphere. The other reagents and solvents were used as supplied, unless stated otherwise.

**Synthesis of Iron Oxide Nanoparticles.** Preparation of the SPIO particles was according to our previous report.<sup>8</sup> Iron(III) chloride hexahydrate (1.081 g, 4 mmol) and iron(II) chloride tetrahydrate (0.3976 g, 2 mmol) were dissolved in water (120 mL). After the addition of oleic acid (0.2 mL) with mechanically stirring at 1000 rpm, 15 mL of aqueous ammonium hydroxylate (28%) was added to the solution all at once. Oleic acid (0.2 mL) was continuously added to the solution in four additions every 5 min with stirring at 1000 rpm at 80 °C. After stirring for 30 min, the resulting dark brown suspension was cooled to room temperature.

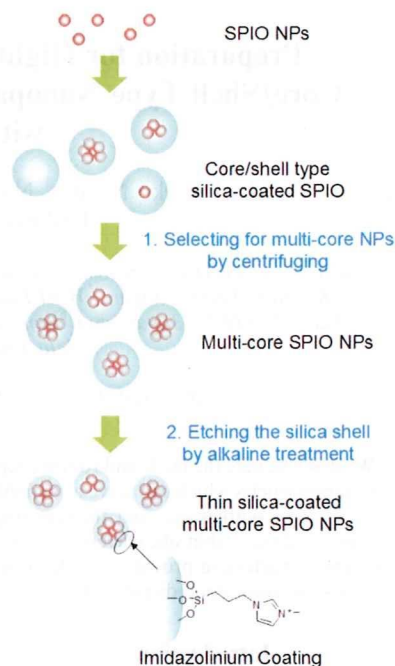
**Silica Coating on the Iron Oxide Nanoparticles.** The preparation of the core/shell type nanoparticles was according to our previous report.<sup>8</sup> In a 50 mL glass vial, 2.3 g of Igepal CO-520 was dissolved in 45 mL of cyclohexane. The solution was mechanically stirring at 700 rpm with sonication for 2 min. After dispersing the SPIO particles, 0.3 mL of the mixture was added to the cyclohexane solution, and then the mixture was stirred at room temperature for 5 min with sonication. The resulting mixture was turned to transparent light brown liquid, and then 0.3 mL of tetraethoxysilane was added. The mixture was gently stirred by hand using a spatula until tetraethoxysilane was completely dissolved, and the mixture was left for 3 days at room temperature to form a thick silica shell.

**Surface Modification on the Core/Shell Nanoparticles.** The surface modification was according to our previous report.<sup>8</sup> In a 1000 mL round-bottom flask, the imidazolium<sup>18</sup> (2.0 g) was dissolved in 200 mL of ethanol. The mixture containing the core/shell particles was rapidly added to the ethanol solution with mechanical stirring at 700 rpm. After the mixture was stirred for 12 h at room temperature, the upper transparent layer was removed, and the light-brown products were separated by centrifuging at 6000 rpm. After washing with 200 mL of methanol three times, the desired core/shell particles were obtained as a brown suspension in methanol.

**Centrifugal Selections.** The particles (100 mg) were dispersed in methanol (10 mL) and centrifuged for 5 min at 25 °C. Recovery yields were calculated from the weight of the precipitations. The number of SPIO cores was counted in TEM images, and the diameters and the number of the SPIO particles were described from the averages of 100 particles in three sets of experiments. The errors represent standard deviation.

**Etching of Silica Layer on the Particles under Alkaline Conditions.** The 1 M sodium hydroxide solution (0.02 mL) was

**Scheme 1. Schematic Illustration for Preparing the Thin Silica-Coated Core/Shell Type Nanoparticles Encapsulating Multiple SPIO Particles**



added to the nanoparticle-dispersed mixture (2 mL, 1 mg/mL), and then the mixture was incubated at 25 °C. The reaction was quenched by the neutralization with HCl. The diameters were calculated as the average of 100 particles in TEM images in three sets of experiments. The errors represent standard deviation.

**MR Imaging.** For the MR imaging and  $T_2$  calculation, all particles were dispersed with ultrasonic waves in Milli-Q water. Agarose XP (Nippon gene) was dissolved in hot Milli-Q water at the concentration of 1 wt %. Nanoparticle dispersions and agarose XP solutions of 250  $\mu\text{L}$  each were vortex-mixed in glass vials and kept cool until their fluidity disappeared. MR imaging of the samples was carried out using a 7 T Unity Inova MR Scanner (Varian, Palo Alto, CA). Coronal images of the samples were obtained with a  $T_2$ -weighted spin-echo sequence. Repetition time (TR) was 3000 ms, echo time (TE) was 40 ms, and the field of view was 40 mm, with an image matrix of  $256 \times 256$  pixels. Slice thickness was 3 mm.

### Results and Discussion

The schematic procedure is summarized in Scheme 1. The assembly of SPIO particles can enhance the magnetism,<sup>9</sup> resulting in clear contrasts in MRI.<sup>3b-d,10</sup> Thus, the first purpose to

(9) (a) Philpse, A. P.; van Bruggen, M. P. B.; Pathmamanoharan, C. *Langmuir* **1994**, *10*, 92–94. (b) Srivastava, S.; Samanta, B.; Jordan, B. J.; Hong, R.; Xiao, Q.; Tuominen, M. T.; Rotello, V. M. *J. Am. Chem. Soc.* **2007**, *129*, 11776–11780. (c) Ditsch, A.; Laibinis, P. E.; Wang, D. I. C.; Hatton, T. A. *Langmuir* **2005**, *21*, 6006–6018. (d) Woo, E.; Ponvel, K. M.; Ahn, I.-S.; Lee, C.-H. *J. Mater. Chem.* **2010**, *20*, 1511–1515. (e) Matsumoto, Y.; Jasanoff, A. *Magn. Reson. Imaging* **2008**, *26*, 994–998. (f) Qiang, Y.; Antony, J.; Sharma, A.; Nutting, J.; Sikes, D.; Meyer, D. *J. Nanopart. Res.* **2006**, *8*, 489–496.

(10) (a) Tromsdorf, U. I.; Bigall, N. C.; Kaul, M. G.; Bruns, O. T.; Nikolic, M. S.; Mollwitz, B.; Sperling, R. A.; Reimer, R.; Hohenberg, H.; Parak, W. J.; Förster, S.; Beisiegel, U.; Adam, G.; Weller, H. *Nano Lett.* **2007**, *7*, 2422–2427. (b) Berret, J.-F.; Schonbeck, N.; Gazeau, F.; El Kharrat, D.; Sandre, O.; Vacher, A.; Airiau, M. *J. Am. Chem. Soc.* **2006**, *128*, 1755–1761. (c) Zhang, C.; Wängler, B.; Morgenstern, B.; Zentgraf, H.; Eisenhut, M.; Untenecker, H.; Krüger, R.; Huss, R.; Seliger, C.; Semmler, W.; Kiessling, F. *Langmuir* **2007**, *23*, 1427–1434. (d) Taboada, E.; Solanas, R.; Rodríguez, E.; Weissleder, R.; Roig, A. *Adv. Funct. Mater.* **2009**, *19*, 2319–2324.



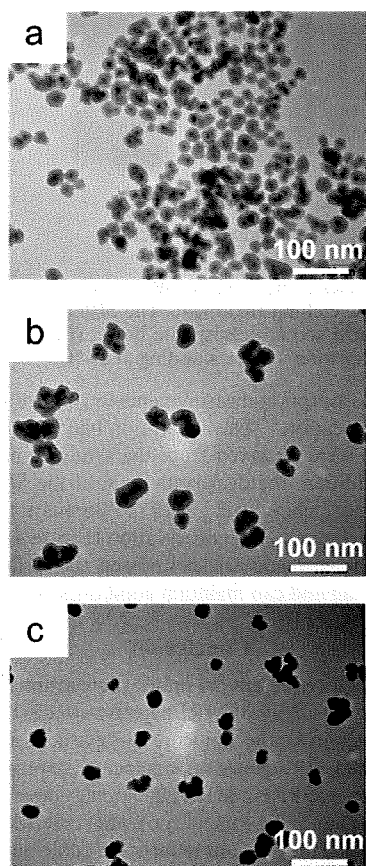


**Figure 1.** TEM images of the core/shell particles (a) before treatments, (b) after the centrifuge selection, and (c) after the alkaline etching.

improve sensitivity of the particles is to encapsulate as many as SPIO particles in the single core/shell particle.<sup>11</sup> The silica-coated SPIO particles were prepared via a reverse-micelle sol-gel technique according to our previous work.<sup>8</sup> We explored the conditions to load the maximum amount of SPIO in reverse micelles, and imidazolium-tethered core/shell nanoparticles were obtained. The thickness of the shell and the number of the SPIO core were counted in TEM images and calculated as an average of 100 particles. The diameter of the SPIO particles at the core was  $\sim 7 \pm 4$  nm, and the dispersed size of the resulting core/shell particles was obtained ( $24.2 \pm 13.0$  nm, Figure 1a).

Initially, we aimed to select multicore particles. The multicore particles were defined as the particles which included at least five SPIOs inside the silica shell because of the difficulty to clearly distinguish two or three SPIO inside the core/shell particles. We executed the centrifugal separation in the isopycnic density media, and the recovery yields were calculated from the amount of the precipitation.<sup>12</sup> By the increase of the rotational speed, the recovery rate of the synthetic particles as a precipitation was improved; however, the proportion of the multicore particles in the products was reduced.<sup>13</sup> It represents that silica and single-core particles were efficiently excluded, and the recovery rate was relatively

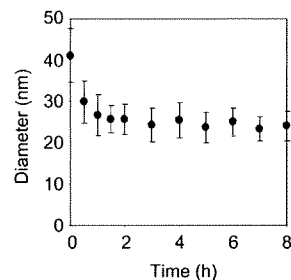


**Figure 2.** Time course of diameter change of the core/shell nanoparticles in 10 mM sodium hydroxide solutions. The diameters of the particles were calculated as the averages of 100 particles in TEM images in the three sets of experiments. Error bars represent the standard deviation.

**Table 1. Components and Diameters of the Core/Shell Particles in the Alkaline Etching Treatment<sup>a</sup>**

incubation time [h]	proportion of the multicore NPs [%] <sup>b</sup>	diameter [nm $\pm$ SD] <sup>b</sup>
0	50	41.1 $\pm$ 14.0
1	51	26.7 $\pm$ 9.9
2	50	25.7 $\pm$ 7.4
4	n.d. <sup>c</sup>	25.5 $\pm$ 8.5
6	n.d. <sup>c</sup>	25.1 $\pm$ 6.9
8	n.d. <sup>c</sup>	24.0 $\pm$ 7.2

<sup>a</sup> Alkaline etching was carried out in 10 mM aqueous sodium hydroxide at 25 °C. <sup>b</sup> All values were calculated as the averages of 100 particles in TEM images. <sup>c</sup> Not determined.

higher at 2200g. Therefore, we adopted this centrifugal condition for next operations. The centrifugal separation was carried out at 2200g three times, and the samples containing  $41 \pm 14$  nm diameter core/shell nanoparticles were obtained (Figure 1b). The elimination of small silica fragments contributed to reducing the range of size dispersion, though the apparent diameter increased by  $\sim 17$  nm by the centrifugal selection.

The relaxation enhancement to water molecules by ferromagnetic materials significantly depends on the distance.<sup>9c,14</sup> Thus, the second purpose is to minimize the thickness of the silica layer on the core/shell particles. Etching treatment was executed in the 10 mM NaOH solution at 25 °C. Figure 2 shows time course of diameter change of the core/shell particles. The average size of the particles decreased by  $\sim 15$  nm and reached a plateau at 2 h. On the other hand, excess alkaline solution collapsed the core/shell particles (Table 1). After the incubation, the surface of the particles was modified with imidazolium, and a well-dispersed suspension can be prepared (Figure 1c). The iron content in the particles was significantly improved by the etching process (Table 2).

Figure 3 shows the  $T_2$ -weighted MR image of the samples containing the SPIO particles at 7 T at 25 °C, and detection limits of the SPIO particles for contrast enhancement were evaluated. The sample without both treatments showed less dark contrast. In contrast, the samples after the selection step showed the enhancement of the proton relaxation. Particularly, the multicore SPIO particles after etching gave much clearer contrast even at  $3.5 \mu\text{g/mL}$  of iron concentration. These results suggest that the sensitivity to create negative contrast was improved at least 7 times larger than

(11) (a) Bromberg, L.; Raduyk, S.; Hatton, T. A. *Anal. Chem.* **2009**, *81*, 5637–5645. (b) Woo, E.; Ponvel, K. M.; Ahn, I.-S.; Lee, C.-H. *J. Mater. Chem.* **2010**, *20*, 1511–1515.

(12) Sun, X.; Tabakman, S. M.; Seo, W.-S.; Zhang, L.; Zhang, G.; Sherlock, S.; Bai, L.; Dai, H. *Angew. Chem., Int. Ed.* **2009**, *48*, 939–942.

(13) See Table S1 in the Supporting Information.

(14) (a) Vogt, C.; Toprak, M. S.; Muhammed, M.; Laurent, S.; Bridot, J.-L.; Müller, R. N. *J. Nanopart. Res.* DOI: 10.1007/s11051-009-9661-7. (b) Yi, D. K.; Lee, S. S.; Papaefthymiou, G. C.; Ying, J. Y. *Chem. Mater.* **2006**, *18*, 614–619. (c) Chen, D.-X.; Sun, N.; Huang, Z.-J.; Cheng, C.-M.; Xu, H.; Gu, H.-C. *J. Magn. Magn. Mater.* **2010**, *322*, 548–556. (d) Zhang, M.; Cushing, B. L.; O'Connor, C. *J. Nanotechnology* **2008**, *19*, 1–5.

Table 2. Properties of the Synthetic Particles

sample	none	selection	selection and etching
Fe component [%]	25	27	42
diameter [nm $\pm$ SD] <sup>a</sup>	24.2 $\pm$ 13.0	41.1 $\pm$ 14.0	25.7 $\pm$ 7.4
shell thickness [nm $\pm$ SD] <sup>a</sup>	17.2 $\pm$ 10.0	34.1 $\pm$ 11.0	18.7 $\pm$ 5.4
$r_2$ [Fe mM <sup>-1</sup> s <sup>-1</sup> ] <sup>b</sup>	179	779	1395
detection limit [ $\mu$ g/mL] <sup>b</sup>	27.5	12.8	4.1

<sup>a</sup>All values were calculated as the averages of 100 particles in TEM images. <sup>b</sup>Detection limits of the synthetic particles were determined from the MR imaging in 7 T at 25 °C.

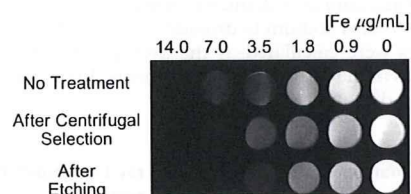


**Figure 3.** MR imaging of various concentration of the core/shell particles. All samples were sealed into 5 mm of glass tubes, and the  $T_2$ -weighted phantom image was taken at 7 T at 25 °C.

that of the sample before treatments. The relaxivity can be improved  $\sim$ 3-fold higher than that of previous system reported as a highly sensitive MRI sensor.<sup>15</sup>

In order to compare the signal enhancement ability, the proton relaxivity ( $r_2$ ) of each SPIO particles was determined from the  $T_2$  measurements (Table 2).<sup>16</sup> The selection by centrifuging can improve the relaxivity four times. In addition, the etching treatment can significantly improve the relaxivity  $\sim$ 2 times compared to the sample before treatments. These data show good agreement with those of Figure 3. These results indicate that the assembly of SPIO to the core and the minimum thickness of the surface in core/shell particles to improve the iron content can realize the significant enhancement of the relaxivity of water tissue around the particles.

The dispersibility of the particles is an important issue for practical usages. We investigated the surface of the SPIO particles after etching. The particles were dissolved in 10 M NaOH aqueous solution, and the supernatants after neutralizing were analyzed

(15) (a) Nasongkla, N.; Bey, E.; Ren, J.; Ai, H.; Khemtong, C.; Guthi, J. S.; Chin, S.-F.; Sherry, A. D.; Boothman, D. A.; Gao, J. *Nano Lett.* **2006**, *6*, 2427–2430. (b) Lee, J.-H.; Huh, Y.-M.; Jun, Y.-W.; Seo, J.-W.; Jang, J.-T.; Song, H.-T.; Kim, S.; Cho, E.-J.; Yoon, H.-G.; Suh, J.-S.; Cheon, J. *Nature Med.* (N. Y., NY, U. S.) **2007**, *13*, 95–99.

(16) The relaxivity  $r_2$  [Fe mM<sup>-1</sup> s<sup>-1</sup>] was calculated from the slope of  $T_2$  dependency on the concentration of iron. See Figure S1 in the Supporting Information.

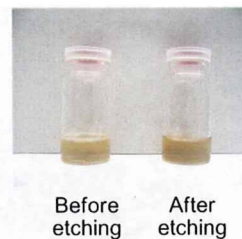


**Figure 4.** Samples containing the SPIO particles before (left) and after (right) the etching treatment. The SPIO particles were dispersed in 50 mM sodium phosphate buffer (pH = 7.0), and the image was taken after 1 week standing at 25 °C.

with UV–vis absorption measurements to confirm the existence of imidazolium cation.<sup>17</sup> The absorption bands from the imidazolium cation were observed from the synthetic particles after etching. In addition, the dispersion state of the SPIO particles with and without etching after 1 week in PBS was not significantly changed from the naked eye observation (Figure 4). These data suggest that the synthetic particles possess the surface modification after etching and can maintain good dispersibility.

## Conclusion

In conclusion, we present the simple preparation technique for improving the sensitivity of MRI negative contrast agents using SPIO. The selection for the multicore nanoparticles and etching of the shell are the key processes for enhancing the proton relaxivity of the silica-coated SPIO in MRI. Our strategy described here can be feasible to enhance the sensitivity of other core/shell type nanoparticles including the previous reports and contribute to improve accuracy in material science as well as in the advanced functional MR imaging methods.

**Acknowledgment.** This study is a part of Kyoto City Collaboration of Regional Entities for the Advancement of Technology Excellence of JST. On the basis of research results, supported in part by a grant-in-aids for Scientific Researches (B) (No. 16310086), and the 21st century COE program, COE for a United Approach to New Material Science, Kyoto University.

**Supporting Information Available:** Experimental details. This material is available free of charge via the Internet at <http://pubs.acs.org>.

(17) Absorption spectra are presented in Figure S2 in the Supporting Information.

(18) The synthetic procedure is described in the Supporting Information.

